

Molecular Insights into Cage Occupancy of Hydrogen Hydrate: A Computational Study

Authors:

Rui Ma, Hong Zhong, Jinxiang Liu, Jie Zhong, Youguo Yan, Jun Zhang, Jiafang Xu

Date Submitted: 2019-12-09

Keywords: molecular dynamics simulation, density functional theory, hydrogen hydrate, stability

Abstract:

Density functional theory calculations and molecular dynamics simulations were performed to investigate the hydrogen storage capacity in the sII hydrate. Calculation results show that the optimum hydrogen storage capacity is ~5.6 wt%, with the double occupancy in the small cage and quintuple occupancy in the large cage. Molecular dynamics simulations indicate that these multiple occupied hydrogen hydrates can occur at mild conditions, and their stability will be further enhanced by increasing the pressure or decreasing the temperature. Our work highlights that the hydrate is a promising material for storing hydrogen.

Record Type: Published Article

Submitted To: LAPSE (Living Archive for Process Systems Engineering)

Citation (overall record, always the latest version):

LAPSE:2019.1290

Citation (this specific file, latest version):

LAPSE:2019.1290-1

Citation (this specific file, this version):


LAPSE:2019.1290-1v1

DOI of Published Version: <https://doi.org/10.3390/pr7100699>

License: Creative Commons Attribution 4.0 International (CC BY 4.0)

Article

Molecular Insights into Cage Occupancy of Hydrogen Hydrate: A Computational Study

Rui Ma ^{1,2}, Hong Zhong ², Jinxiang Liu ^{1,*} , Jie Zhong ³, Youguo Yan ², Jun Zhang ² and Jiafang Xu ^{4,*}¹ School of Physics and Technology, University of Jinan, Jinan 250022, China; microrean@163.com² School of Materials Science and Engineering, China University of Petroleum, Qingdao 266580, China; zhongh827@yeah.net (H.Z.); yyg@upc.edu.cn (Y.Y.); sps_zhang@hotmail.com (J.Z.)³ Department of Chemistry, University of Nebraska-Lincoln, Lincoln, NE 68588, USA; dynamic.zhong@outlook.com⁴ School of Petroleum Engineering, China University of Petroleum, Qingdao 266580, China

* Correspondence: sps_liujx@ujn.edu.cn (J.L.); xjiafang@upc.edu.cn (J.X.)

Received: 29 August 2019; Accepted: 30 September 2019; Published: 3 October 2019



Abstract: Density functional theory calculations and molecular dynamics simulations were performed to investigate the hydrogen storage capacity in the sII hydrate. Calculation results show that the optimum hydrogen storage capacity is ~5.6 wt%, with the double occupancy in the small cage and quintuple occupancy in the large cage. Molecular dynamics simulations indicate that these multiple occupied hydrogen hydrates can occur at mild conditions, and their stability will be further enhanced by increasing the pressure or decreasing the temperature. Our work highlights that the hydrate is a promising material for storing hydrogen.

Keywords: hydrogen hydrate; stability; density functional theory; molecular dynamics simulation

1. Introduction

Hydrogen has attracted great attention as an alternative renewable and sustainable transportation fuel [1,2]. For the practice applications, a mass of materials have been studied for hydrogen storage, including nanostructured materials, carbon-based materials and metal hydrides [3–5]. However, it is still challenging to develop highly efficient hydrogen storage materials. In recent decades, clathrate hydrates have been proposed as a promising technology for hydrogen storage [6–10]. Clathrate hydrates are solid compounds in which small gas molecules are trapped in the hydrogen-bonded cages of water molecules. There are three most common crystalline structures of hydrates: sI, sII, and sH [11,12]. Hydrogen favors to form sII hydrate, which contains sixteen small 5^{12} (12 pentagonal faces) cages and eight large $5^{12}6^4$ (12 pentagonal and four hexagonal faces) cages in one unit cell.

Mao et al. [6,13] experimentally synthesized sII hydrogen hydrate at about 200 Mpa and suggested that the cage occupancy is two H_2 molecules in 5^{12} cage and four H_2 molecules in $5^{12}6^4$ cages. Patchkovskii et al. [14] theoretically investigated the stability of pure hydrogen hydrate and indicated that the cage occupation of 5^{12} and $5^{12}6^4$ cages is 2.00 and 3.96 H_2 molecules, respectively. They also demonstrated that pure hydrogen hydrates are stable at 2.5 MPa and 150 K. Quantum dynamics [15,16], path integral molecular dynamics [17], and the force-matching method [18] suggested that the maximum occupancy of $5^{12}6^4$ cage is four hydrogen molecules at low temperatures. Raman spectra study [19] predicted that 5^{12} cage can be doubly occupied by H_2 molecules. Molecular dynamics simulations [20] indicated that H_2 molecules can migrate from the 5^{12} cages to neighboring cages for hydrogen hydrate with double small-cage occupation. Papadimitriou et al. [21] suggested that the hydrogen occupancy of $5^{12}6^4$ cages is considerably influenced by the lattice constant, and Brumby et al. [22] observed that a

small number of the large cages could be occupied by five H₂ molecules. Willow and Xantheas [10] demonstrated that 5¹² and 5¹²6² cages can accommodate three and six H₂ molecules, respectively. Moreover, Lokshin et al. [23] demonstrated that 5¹² cages are singly occupied, which 5¹²6⁴ cages can be occupied by 2–4 H₂ molecules depending on pressure or temperature. Inerbaev et al. [24] suggested that 5¹²6⁴ cages are quadruply occupied by H₂ molecules at 200 MPa and 190 K, and the cage occupancy decreases with the increase of the temperature. Raman measurements [25] suggested that the occupancy of 5¹²6⁴ cages is less than or equal to two H₂ molecules. Therefore, the cage occupancy of the pure hydrogen hydrate is still controversial [26,27], and great efforts should be made to address this question.

On the other hand, high pressures are needed to form pure hydrogen hydrates, which is not economically feasible and leads to the research of the mixed hydrogen hydrates at lower pressures [28–33]. For example, Florusse et al. [34] suggested that tetrahydrofuran can stabilize the hydrogen hydrates at 5.0 MPa and 279.6 K, and Lee's group [7] reported that the storage capacity is about 4.0 wt% at 12 MPa for the binary hydrogen hydrate. In addition, multiple H₂ molecules can be loaded into 5¹² and 5¹²6⁴ cages through the replacement of N₂ hydrate by H₂ gas at moderate condition [9]. Nevertheless, the storage capacity of hydrates is compromised because the additional molecules occupy the large cages instead of hydrogen clusters.

In this paper, we carried out density functional theory calculations and molecular dynamics simulations to study the hydrogen storage properties of hydrogen hydrate. Our results showed that the optimum storage capacity of the pure hydrogen hydrate can reach up to 5.6 wt%. Moreover, these multiply occupied hydrogen hydrates can occur at mild pressure and low temperature, which would be helpful to inspire new experiments for synthesizing hydrogen hydrate with high storage capacity.

2. Computational Details

Firstly, we built a primitive cell (11.89 × 11.89 × 11.89 Å³) of sII hydrate [35], which consists of four 5¹² and two 5¹²6⁴ cages. After filling a hydrogen cluster of (H₂)_{n = 1–6} and (H₂)_{m = 1–8} into the 5¹² cage and the 5¹²6² cage, respectively, we carried out the geometry optimization for the hydrates with three-dimensional periodic boundary conditions, in which the coordinates of atoms were adjusted so that the energy of the structure is brought to a stationary point. There are no imaginary frequencies in vibrational analysis, presenting the most stable structures. The calculations were implemented through DMol³ program. The Becke–Lee–Yang–Parr [36,37] (BLYP) exchange-correlation functional and the double numerical plus polarization, with addition of diffuse functions (DNP+) basis set [38] were applied. The Tkatchenko–Scheffler approach [39] was used for the dispersion correction. The convergence criteria is 1 × 10^{−5} Ha for the total energy, 0.002 Ha/Å for forces, 0.005 Å for displacement, and 1 × 10^{−6} Ha for SCF interactions.

The stability of the hydrates was characterized by the cohesive energy per water molecule (E_{coh}) that was computed as following [40]:

$$E_{coh} = \frac{[x \cdot E_{hydrogen} + 34 \cdot E_{water}] - E_{hydrate}}{34} \quad (1)$$

where $E_{hydrogen}$ denotes the energy of the hydrogen molecule, E_{water} denotes the energy of the water molecule, $E_{hydrate}$ denotes the energy of the hydrate, and x denotes the number of hydrogen molecules. Zero-point energy is added to the electronic energy when computing and comparing above energies. Further, global reactivity parameters such as the electronegativity (χ) [41], global hardness (η) [42] and electrophilicity index (ω) [43] were calculated by the following equations:

$$\chi = -\left(\frac{\partial E}{\partial N}\right)_{v(\vec{r})} \quad (2)$$

$$\eta = \left(\frac{\partial^2 E}{\partial N^2}\right)_{v(\vec{r})} = \left(\frac{\partial \mu}{\partial N}\right)_{v(\vec{r})} \quad (3)$$

$$\omega = \frac{\chi^2}{2\eta} \quad (4)$$

where E represents the total energy, N represents number of electrons, and $v(\vec{r})$ represents external potential. The binding ability of single H_2 molecule within the hydrate was evaluated by the interaction energy (E_{int}), as [8]

$$E_{int} = (E_{H_2} + E_{residual}) - E_{hydrate} \quad (5)$$

where E_{H_2} is the energy of single H_2 molecule, and $E_{residual}$ is the energy of the hydrate with one lost H_2 molecule. The distortion of the water lattice was characterized by the deformation energy (E_{def}), as [44]

$$E_{def} = E_{cage} - E_{opt-cage} \quad (6)$$

where E_{cage} is the energy of the hydrate without hydrogen molecules at its geometry to accommodate hydrogen clusters, and $E_{opt-cage}$ is the energy of the hydrate without hydrogen molecules at its optimized geometry.

Subsequently, we chose the most thermodynamically stable structure of pure hydrogen hydrates, with two H_2 molecules in 5^{12} cages and five in $5^{12}6^4$ cages, and investigated the effect of temperature and pressure on its stability. By using a large-sized unit cell ($23.78 \times 23.78 \times 23.78 \text{ \AA}^3$) and three-dimensional periodic boundary conditions, molecular dynamics (MD) simulations were carried out in the constant-pressure and constant-temperature (NPT) ensemble as implemented in the Discover program modules of Materials Studio developed by Accelrys Inc. [45] Initially, the atomic positions of water molecules were frozen and a 200-ps simulation was carried out. Then, the coordinate constraints of water molecules were removed and another 100-ps simulation was performed. The Andersen thermostat [46] was used to control the temperature and the Berendsen barostat [47] was used to control the pressure. The Ewald summation method [48] and COMPASS force field [49–51] was used for the energy calculation, and the time step was set 1.0 fs.

The diffusion motion of the hydrogen hydrate was characterized by the mean square displacement (MSD), which was calculated by the following equation:

$$MSD = \left\langle \left(\vec{r}_i(t) - \vec{r}_i(0) \right)^2 \right\rangle \quad (7)$$

where $\vec{r}_i(t) - \vec{r}_i(0)$ is the shift distance of molecules in an interval t , and the angular brackets indicate an ensemble average. According on the Debye theory [52], the diffusion coefficient (D) can be obtained by the equation:

$$D = \frac{MSD}{6t} \quad (8)$$

3. Results and Discussion

3.1. The Hydrate Stability with Respect to the Hydrogen Occupancy

For the multiple hydrogen hydrate, we considered complexes encapsulated with a $(H_2)_{n=1-6}$ cluster in the small cage and simultaneously with a $(H_2)_{m=1-8}$ cluster in the large cage. The calculated cohesive energies are shown in Figure 1. It can be seen that the optimum occupancy of 5^{12} cage is two H_2 molecules, because the hydrate has the highest stability. For the large cage, when it encapsulates five or six H_2 molecules, the hydrate exhibits the highest stability. Encapsulating the excess H_2 molecules in $5^{12}6^2$ cage will decrease the stability of the hydrate. Encouragingly, the highest cohesive energy occurs when two H_2 molecules are encapsulated in 5^{12} cage and simultaneously five in $5^{12}6^2$ cage, leading to the hydrogen storage capacity of ~5.6 wt%.

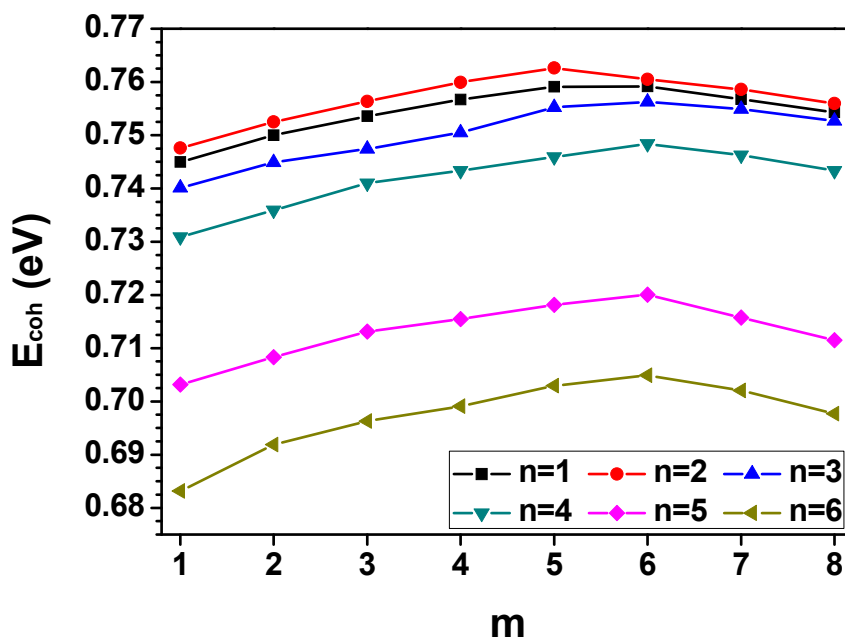


Figure 1. The cohesive energy of the hydrogen hydrate with a cluster of $(\text{H}_2)_{n=1-6}$ in the small cage and $(\text{H}_2)_{m=1-8}$ in the large cage. The atomic coordinates of the hydrates are given in the Supplementary Materials.

Figure 2 shows the global hardness (η), the electrophilicity index (ω), the interaction energy (E_{int}) and the deformation energy (E_{def}) for the hydrogen hydrates. As compared with the hydrate without encapsulating H_2 molecules ($\eta = 3.355$ eV), the single occupancy in the small and large cages results in a large hardness (3.437 eV) of the hydrate. This suggests that the singly occupied hydrate has a potential to resist changes in its electron number and distribution, exhibiting the high chemical stability. It can be attributed to the fact that the interactions between H_2 molecules and the host lattice stabilize the hydrate. Upon adding a second H_2 molecule in the small cage, the hardness of the hydrate further increases to 3.487 eV, implying that this doubly occupied hydrate will be less polarizable if electron transfer or rearrangement is necessary for the reaction. By sequentially increasing the number of H_2 molecules in the large cage, the hardness of the hydrogen hydrates firstly increases and then decreases, featuring a maximum value (3.608 eV) at $m = 5$. This confirms that when the small and the large cages accommodate two and five H_2 molecules, respectively, the hydrogen hydrate has the highest stability. Figure 2b shows that the singly occupied hydrate has a smaller electrophilicity index than the hydrate without H_2 molecules (2.264 eV vs. 2.365 eV), indicating that the electron transfer process will be less energetically favorable in the former. As for the double occupancy in the small cage, the propensity of the hydrate to soak up electrons becomes poorer due to its smaller electrophilicity index (2.192 eV), corresponding to the higher chemical stability. Moreover, the electrophilicity index decreases when the number of H_2 molecules in the large cage increases to five. These results match well with the aforementioned the cohesive energies, confirming that the optimum storage capacity of sII hydrate should be ~ 5.6 wt% H_2 .

For the singly occupied hydrate, the interaction energy per H_2 molecule in the small and large cages was 0.168 eV and 0.137 eV, respectively. For the double occupancy in the small cage, the interaction energy slightly decreased to 0.160 eV in the small cage, and maintained 0.137 eV in the large cage. This indicates that the small cage can accommodate two H_2 molecules, without significantly decreasing the binding ability of the H_2 molecule. From Figure 2c, it can be seen that the interaction energy gradually increases as the number of H_2 molecules in the large cage increases from one to five. While adding an excess H_2 molecule, the interaction energy declines, suggesting that the optimum occupancy of the large cage is five H_2 molecules.

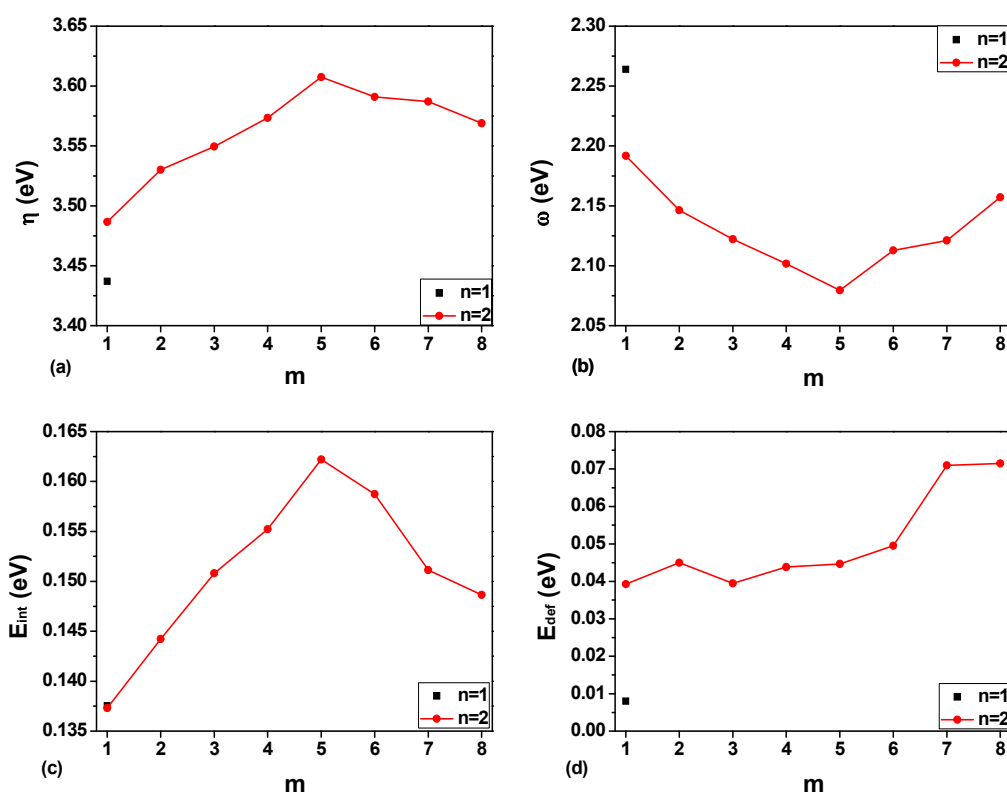


Figure 2. The global hardness (a), electrophilicity index (b), interaction energy of H_2 molecule in large cage (c), and deformation energy (d) for the hydrogen hydrates with a cluster of $(H_2)_{n=1-2}$ in the small cage and $(H_2)_{m=1-8}$ in the large cage.

Figure 2d shows that the deformation energy of the host lattice is 0.008 eV for the single occupancy of the cage, but it increases to 0.039 eV for the double occupancy in the small cage. This indicates that the small cage will become slightly distorted to accommodate two H_2 molecules. On the other hand, when the large cage accommodates 1–5 H_2 molecules, the deformation energy fluctuates around ~ 0.042 eV. While the deformation energy greatly increases as the large cage encapsulates the excess H_2 molecules. In addition, we analyzed the radial distribution functions (RDFs) of oxygen atoms of water molecules in hydrogen hydrates with different cage occupancy. From Figure 3, it can be seen that the RDF for the hydrate without encapsulating H_2 molecules has a sharp and narrow peak at ~ 2.710 Å, corresponding to the hydrogen bond length of water molecules [53]. The second peak at ~ 4.350 Å indicates the tetrahedral structure of water molecules in the hydrate. In the case of the single occupancy, the positions of two peaks have no change, while the intensity of first peak becomes relatively small. Moreover, RDFs of the hydrates exhibit the same trend when a $(H_2)_2$ cluster resides in the small cage and a $(H_2)_{m=1-5}$ cluster in the large cage. In contrast, the first peak is significantly broadened and weakened by sequentially increasing the number of H_2 molecules in the large cage, corresponding to the considerable deformation of the host lattice. This result further suggests that the optimum cage capacity of the large cage is five H_2 molecules.

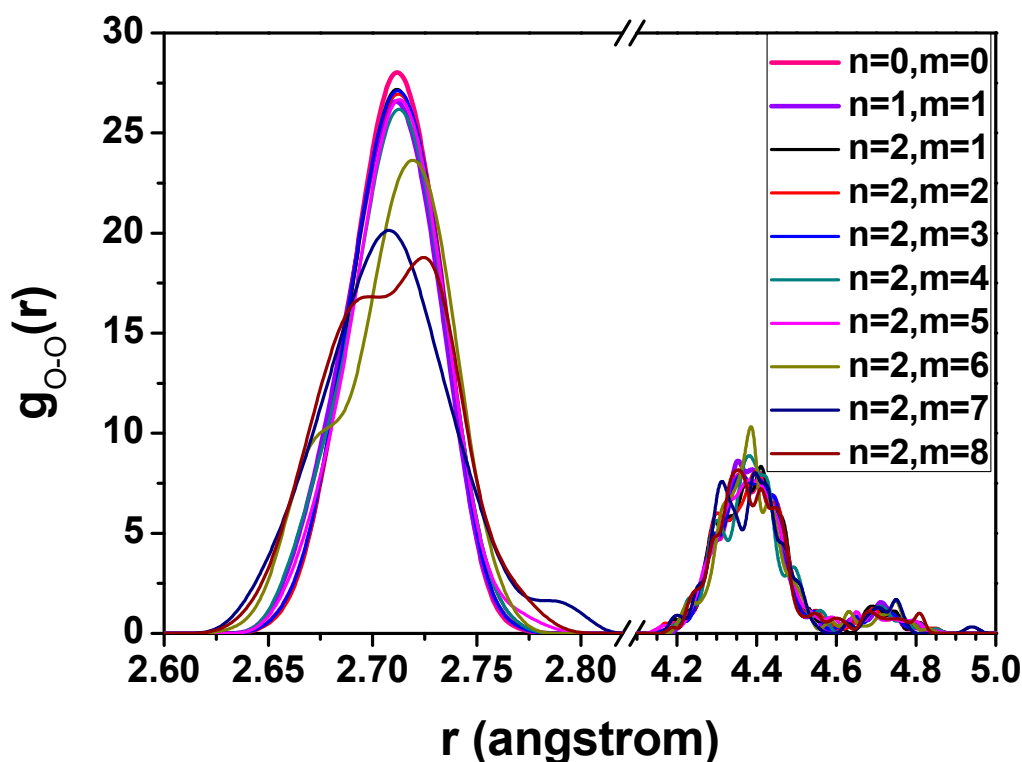


Figure 3. Radial distribution functions of oxygen atoms of water molecules in the hydrogen hydrates with a cluster of $(\text{H}_2)_{n=0-2}$ in the small cage and $(\text{H}_2)_{m=0-8}$ in the large cage.

3.2. Effect of Pressure on the Hydrate Stability

Above studies mainly investigated the thermodynamic stability of the hydrogen hydrate as a function of the H_2 occupancy, which were conducted at 0 K in vacuum. However, pressure and temperature can significantly affect the hydrate stability. Therefore, in the following work, we chose the most thermodynamically stable structure of the hydrogen hydrates, which has two H_2 molecules in 5^{12} cage and five in $5^{12}6^2$ cage, and investigated the effect of temperature and pressure on its stability.

Figure 4 shows the equilibrium configurations of the dynamic trajectories for the hydrogen hydrate at 250 K and at the pressure of 200, 100, 20, and 5 MPa, respectively. Clearly, the hydrate can maintain its structure at 200 MPa, despite of little deformation caused by the thermal and structural fluctuations. As the pressure decreases, the deformation of the hydrate structure becomes more significant; however, the crystal structure can still be observed at 20 MPa. In contrast, at 5 MPa the positions of water molecules are considerably changed and the hydrate structure almost disappears during the dynamics.

Figure 5a shows RDFs of oxygen atoms of water molecules in hydrate at four different pressures. There are two evident peaks at ~ 2.710 Å and ~ 4.430 Å, respectively, indicating the tetrahedral bonding structure of water molecules. However, as the pressure decreases, the intensity of the first peak decreases, suggesting that the hydrogen bonds become weak. Meanwhile, the second peak becomes broadened and shifts to the right, implying that the hydrate has a large deformation. Further, we characterized the diffusion of the hydrate at different pressure. Figure 5b shows the mean square displacement (MSD) of molecules in the hydrogen hydrate. As the pressure decreases, MSD increases more quickly and has a larger slope, corresponding to the rapid diffuse of molecules in the hydrate. The diffusion coefficient is 0.857 , 1.033 , 1.329 , and 1.992×10^{-5} cm^2/s for the hydrate at 200, 100, 20, and 5 MPa, respectively. This indicates that the hydrate will exhibit significant diffusive motion at low pressure, and thus has a less stability.

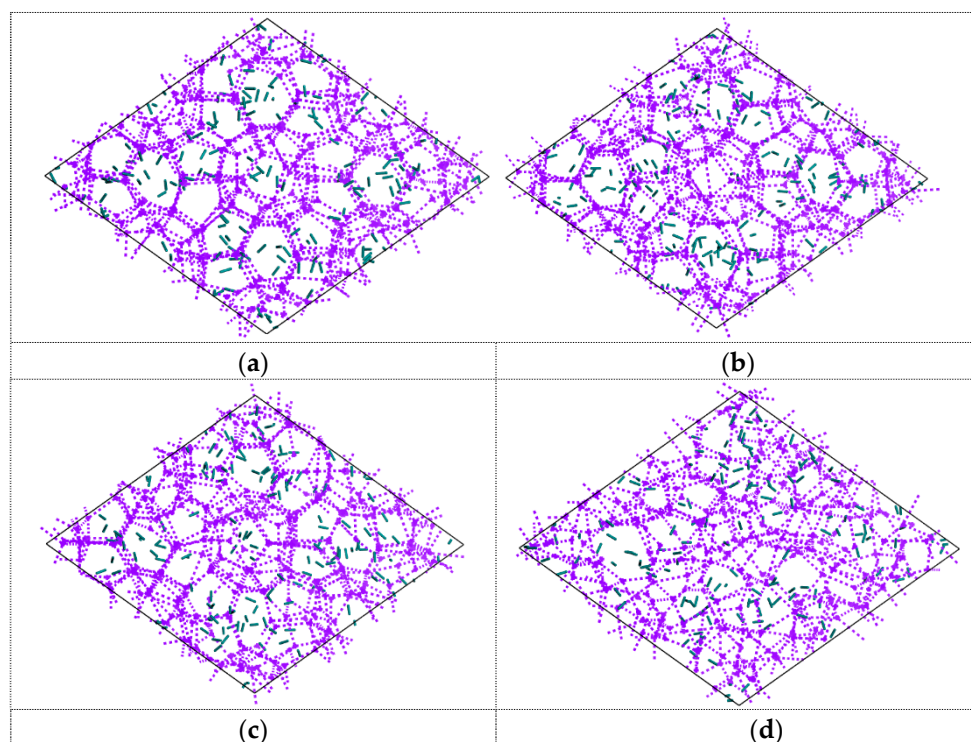


Figure 4. The final configurations of 100-ps MD trajectories of the hydrogen hydrate at 250 K: (a) 200 MPa, (b) 100 MPa, (c) 20 MPa, and (d) 5 MPa. The violet lines represent the hydrogen bonds between water molecules in the hydrate. Water molecules are not shown and hydrogen molecules are shown in dark-cyan stick model.

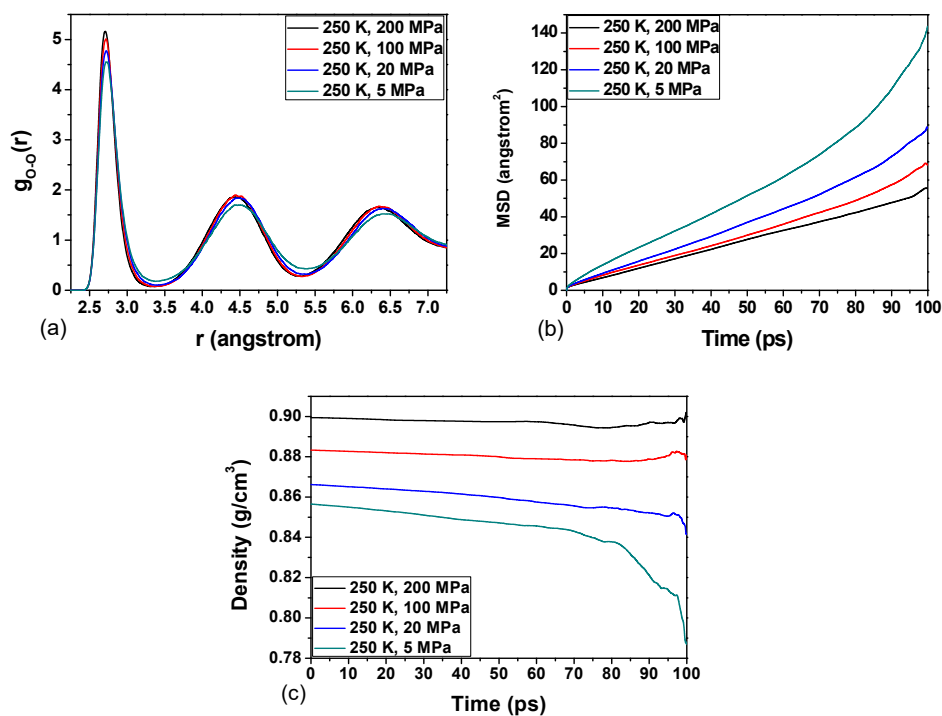


Figure 5. (a) Radial distribution functions of oxygen atoms of water molecules at 250 K and 200 MPa, 100 MPa, 20 MPa, and 5 MPa, respectively. (b) Mean square displacement of molecules in the hydrate at 250 K and 200 MPa, 100 MPa, 20 MPa, and 5 MPa, respectively. (c) Time evolution of the density of the hydrate at 250 K and 200 MPa, 100 MPa, 20 MPa, and 5 MPa, respectively.

For the thermodynamically stable structure (at 0 K), the hydrate has the density of about 0.906 g/cm^3 , while in a thermal and structural fluctuating environment its density decreases because of the enlarged lattice parameters. From Figure 5c, the density of the hydrate decrease to 0.897 g/cm^3 at 200 MPa, 0.880 g/cm^3 at 100 MPa, and 0.859 g/cm^3 at 20 MPa, but these values remain unchanged during the simulations. In contrast, at 5 MPa the hydrate density decreases from 0.849 g/cm^3 to 0.787 g/cm^3 at 100 ps, implying that the hydrate can not maintain its structure at 5 MPa.

3.3. Effect of Temperature on the Hydrate Stability

Figure 6 shows the dynamically relaxed configurations of the hydrogen hydrate at mild pressure (20 MPa) and at temperatures of 280, 250, 200, and 150 K, respectively. It can be seen that the crystalline structure of the hydrate disappears at 280 K. When the temperature decreases, the hydrate becomes more stable and keeps its structure at the temperature of less than 200 K.

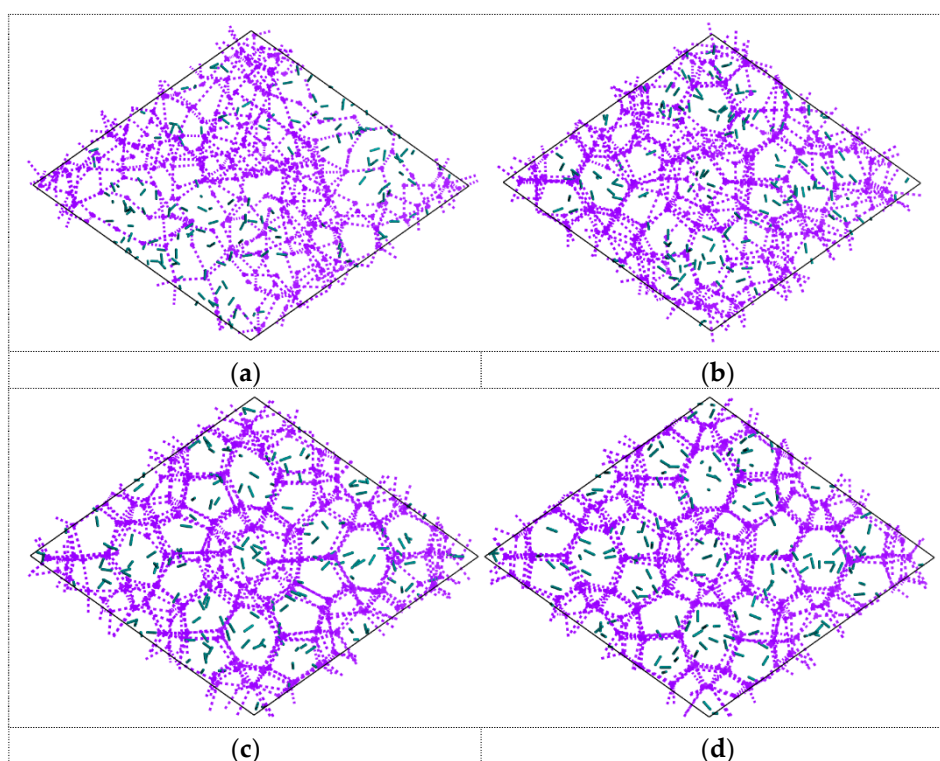


Figure 6. The final configurations of 100-ps MD trajectories of the hydrogen hydrate at 20 MPa: (a) 280 K, (b) 250 K, (c) 200 K, and (d) 150 K. The violet lines represent the hydrogen bonds between water molecules in the hydrate. Water molecules are not shown and hydrogen molecules are shown in dark-cyan stick model.

From Figure 7a, it can be seen that there are two significant peaks at $\sim 2.710 \text{ \AA}$ and $\sim 4.450 \text{ \AA}$, respectively, also implying the tetrahedral bonding structure of water molecules. The intensity of two peaks increases with the decrease of the temperature, suggesting that the stability of the hydrate is improved at the low temperature. Figure 7b shows that the hydrate diffuses significantly at 280 K, while it exhibits less diffusive at 250, 200, and 150 K. It implies that the hydrate will maintain its crystalline structure when the temperature decreases to 250 K. The diffusion coefficient of the hydrate is $4.189, 1.033, 0.682,$ and $0.514 \times 10^{-5} \text{ cm}^2/\text{s}$ at 280 K, 250 K, 200 K, and 150 K, respectively. It further demonstrates that the hydrate become less diffusive as the temperature decreases. Further, Figure 7c indicates that the initial density of the hydrate is $\sim 0.830 \text{ g/cm}^3$ at 280 K and decreases to 0.647 g/cm^3 during the simulation. At 250 K, 200 K and 150 K, the density is about $0.862, 0.875,$ and 0.884 g/cm^3 ,

respectively, fluctuating little during the dynamics. Accordingly, the hydrogen hydrate should exist at mild pressure and low temperatures.

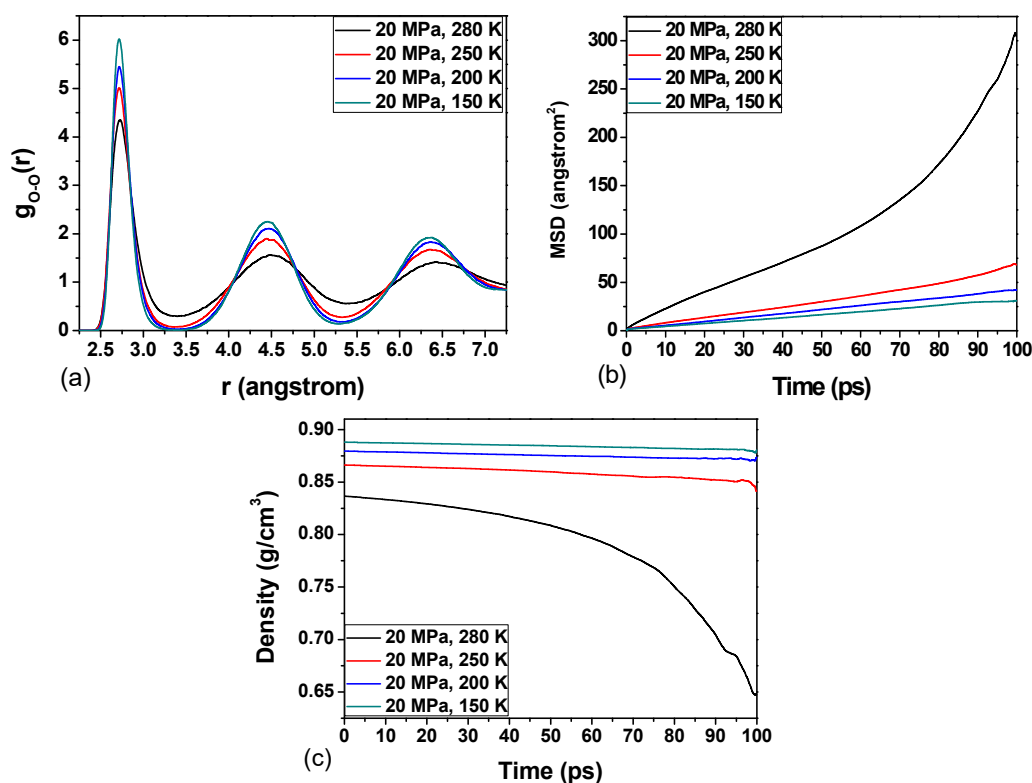


Figure 7. (a) Radial distribution functions of oxygen atoms of water molecules at 20 MPa and 280 K, 250 K, 200 K, and 150 K, respectively. (b) Mean square displacement of molecules in the hydrate at 20 MPa and 280 K, 250 K, 200 K, and 150 K, respectively. (c) Time evolution of the density of the hydrate at 20 MPa and 280 K, 250 K, 200 K, and 150 K, respectively.

4. Conclusions

In this work, we carried out density functional theory calculations and molecular dynamics simulations to investigate the thermodynamic and dynamic stability of sII hydrogen hydrate. Our calculations show that the optimum cage occupancy is two and five H₂ molecules for the small and large cages, respectively, leading to the hydrogen storage capacity of ~5.6 wt%. Through molecular dynamics simulations, we found that the hydrogen hydrate can occur under the conditions of the mild pressure (>20 MPa) and the low temperature (<250 K). Despite of the unclear formation conditions, our results highlight that clathrate hydrates should be a satisfied method for the hydrogen storage.

Supplementary Materials: The following are available online at <https://www.mdpi.com/2227-9717/7/10/699/s1>.

Author Contributions: Investigation, R.M. and H.Z.; supervision, J.L. and J.Z. (Jun Zhang); writing—original draft, J.L.; writing—review & editing, J.Z. (Jie Zhong), Y.Y. and J.X.

Funding: This work was supported by National Natural Science Foundation of China [Grant numbers 11974144 and 11504133].

Conflicts of Interest: The authors declare no conflict of interest.

References

1. Dresselhaus, M.S.; Thomas, I.L. Alternative energy technologies. *Nature* **2001**, *414*, 332–337. [[CrossRef](#)] [[PubMed](#)]
2. Getman, R.B.; Bae, Y.-S.; Wilmer, C.E.; Snurr, R.Q. Review and analysis of molecular simulations of methane, hydrogen, and acetylene storage in metal–organic frameworks. *Chem. Rev.* **2012**, *112*, 703–723. [[CrossRef](#)] [[PubMed](#)]
3. Schlapbach, L.; Züttel, A. Hydrogen-storage materials for mobile applications. *Nature* **2001**, *414*, 353–358. [[CrossRef](#)] [[PubMed](#)]
4. Jena, P. Materials for hydrogen storage: Past, present, and future. *J. Phys. Chem. Lett.* **2011**, *2*, 206–211. [[CrossRef](#)]
5. Schüth, F. Encapsulation strategies in energy conversion materials. *Chem. Mater.* **2014**, *26*, 423–434. [[CrossRef](#)]
6. Mao, W.L.; Mao, H.-K. Hydrogen storage in molecular compounds. *Proc. Natl. Acad. Sci. USA* **2004**, *101*, 708–710. [[CrossRef](#)]
7. Lee, H.; Lee, J.-W.; Kim, D.Y.; Park, J.; Seo, Y.-T.; Zeng, H.; Moudrakovski, I.L.; Ratcliffe, C.I.; Ripmeester, J.A. Tuning clathrate hydrates for hydrogen storage. *Nature* **2005**, *434*, 743–746. [[CrossRef](#)]
8. Román-Pérez, G.; Moaied, M.; Soler, J.M.; Yndurain, F. Stability, adsorption, and diffusion of CH₄, CO₂, and H₂ in clathrate hydrates. *Phys. Rev. Lett.* **2010**, *105*, 145901. [[CrossRef](#)]
9. Lu, H.; Wang, J.; Liu, C.; Ratcliffe, C.I.; Becker, U.; Kumar, R.; Ripmeester, J. Multiple H₂ occupancy of cages of clathrate hydrate under mild conditions. *J. Am. Chem. Soc.* **2012**, *134*, 9160–9162. [[CrossRef](#)]
10. Willow, S.Y.; Xantheas, S.S. Enhancement of hydrogen storage capacity in hydrate lattices. *Chem. Phys. Lett.* **2012**, *525*, 13–18. [[CrossRef](#)]
11. Sloan, E.D. Fundamental principles and applications of natural gas hydrates. *Nature* **2003**, *426*, 353–363. [[CrossRef](#)] [[PubMed](#)]
12. Zhu, J.; Du, S.; Yu, X.; Zhang, J.; Xu, H.; Vogel, S.C.; Germann, T.C.; Francisco, J.S.; Izumi, F.; Momma, K.; et al. Encapsulation kinetics and dynamics of carbon monoxide in clathrate hydrate. *Nat. Commun.* **2014**, *5*, 4128. [[CrossRef](#)] [[PubMed](#)]
13. Mao, W.L.; Mao, H.-k.; Goncharov, A.F.; Struzhkin, V.V.; Guo, Q.; Hu, J.; Shu, J.; Hemley, R.J.; Somayazulu, M.; Zhao, Y. Hydrogen clusters in clathrate hydrate. *Science* **2002**, *297*, 2247–2249. [[CrossRef](#)]
14. Patchkovskii, S.; Tse, J.S. Thermodynamic stability of hydrogen clathrates. *Proc. Natl. Acad. Sci. USA* **2003**, *100*, 14645–14650. [[CrossRef](#)] [[PubMed](#)]
15. Sebastianelli, F.; Xu, M.; Bačić, Z. Quantum dynamics of small H₂ and D₂ clusters in the large cage of structure II clathrate hydrate: Energetics, occupancy, and vibrationally averaged cluster structures. *J. Chem. Phys.* **2008**, *129*, 244706. [[CrossRef](#)]
16. Ranieri, U.; Koza, M.M.; Kuhs, W.F.; Gaal, R.; Klotz, S.; Falenty, A.; Wallacher, D.; Ollivier, J.; Gillet, P.; Bove, L.E. Quantum dynamics of H₂ and D₂ confined in hydrate structures as a function of pressure and temperature. *J. Phys. Chem. C* **2019**, *123*, 1888–1903. [[CrossRef](#)]
17. Witt, A.; Sebastianelli, F.; Tuckerman, M.E.; Bačić, Z. Path integral molecular dynamics study of small H₂ clusters in the large cage of structure II clathrate hydrate: Temperature dependence of quantum spatial distributions. *J. Phys. Chem. C* **2010**, *114*, 20775–20782. [[CrossRef](#)]
18. Burnham, C.J.; Futera, Z.; English, N.J. Study of hydrogen-molecule guests in type II clathrate hydrates using a force-matched potential model parameterised from ab initio molecular dynamics. *J. Chem. Phys.* **2018**, *148*, 102323. [[CrossRef](#)]
19. Wang, J.; Lu, H.; Ripmeester, J.A. Raman spectroscopy and cage occupancy of hydrogen clathrate hydrate from first-principle calculations. *J. Am. Chem. Soc.* **2009**, *131*, 14132–14133. [[CrossRef](#)]
20. Gorman, P.D.; English, N.J.; MacElroy, J.M.D. Dynamical cage behaviour and hydrogen migration in hydrogen and hydrogen-tetrahydrofuran clathrate hydrates. *J. Chem. Phys.* **2012**, *136*, 044506. [[CrossRef](#)]
21. Papadimitriou, N.I.; Tsimpanogiannis, I.N.; Economou, I.G.; Stubos, A.K. The effect of lattice constant on the storage capacity of hydrogen hydrates: A Monte Carlo Study. *Mol. Phys.* **2016**, *114*, 2664–2671. [[CrossRef](#)]
22. Brumby, P.E.; Yuhara, D.; Hasegawa, T.; Wu, D.T.; Sum, A.K.; Yasuoka, K. Cage occupancies, lattice constants, and guest chemical potentials for structure II hydrogen clathrate hydrate from Gibbs ensemble Monte Carlo simulations. *J. Chem. Phys.* **2019**, *150*, 134503. [[CrossRef](#)] [[PubMed](#)]

23. Lokshin, K.A.; Zhao, Y.; He, D.; Mao, W.L.; Mao, H.-K.; Hemley, R.J.; Lobanov, M.V.; Greenblatt, M. Structure and dynamics of hydrogen molecules in the novel clathrate hydrate by high pressure neutron diffraction. *Phys. Rev. Lett.* **2004**, *93*, 125503. [[CrossRef](#)] [[PubMed](#)]
24. Inerbaev, T.M.; Belosludov, V.R.; Belosludov, R.V.; Sluiter, M.; Kawazoe, Y. Dynamics and equation of state of hydrogen clathrate hydrate as a function of cage occupation. *Comput. Mater. Sci.* **2006**, *36*, 229–233. [[CrossRef](#)]
25. Del Rosso, L.; Celli, M.; Ulivi, L. Raman measurements of pure hydrogen clathrate formation from a supercooled hydrogen–water solution. *J. Phys. Chem. Lett.* **2015**, *6*, 4309–4313. [[CrossRef](#)]
26. English, N.J.; MacElroy, J.M.D. Perspectives on molecular simulation of clathrate hydrates: Progress, prospects and challenges. *Chem. Eng. Sci.* **2015**, *121*, 133–156. [[CrossRef](#)]
27. Rasoolzadeh, A.; Shariati, A. Hydrogen hydrate cage occupancy: A key parameter for hydrogen storage and transport. *Fluid Phase Equilib.* **2019**, *494*, 8–20. [[CrossRef](#)]
28. Sugahara, T.; Haag, J.C.; Prasad, P.S.R.; Warntjes, A.A.; Sloan, E.D.; Sum, A.K.; Koh, C.A. Increasing hydrogen storage capacity using tetrahydrofuran. *J. Am. Chem. Soc.* **2009**, *131*, 14616–14617. [[CrossRef](#)]
29. Chapoy, A.; Anderson, R.; Tohidi, B. Low-pressure molecular hydrogen storage in semi-clathrate hydrates of quaternary ammonium compounds. *J. Am. Chem. Soc.* **2007**, *129*, 746–747. [[CrossRef](#)]
30. Cai, J.; Tao, Y.-Q.; von Solms, N.; Xu, C.-G.; Chen, Z.-Y.; Li, X.-S. Experimental studies on hydrogen hydrate with tetrahydrofuran by differential scanning calorimeter and in-situ Raman. *Appl. Energ.* **2019**, *243*, 1–9. [[CrossRef](#)]
31. Liu, J.; Yan, Y.; Chen, G.; Hou, J.; Yan, Y.; Liu, H.; Li, S.; Zhang, J. Prediction of efficient promoter molecules of sh hydrogen hydrate: An ab initio study. *Chem. Phys.* **2019**, *516*, 15–21. [[CrossRef](#)]
32. Kaur, S.P.; Ramachandran, C.N. Hydrogen-tetrahydrofuran mixed hydrates: A computational study. *Int. J. Hydrogen Energy* **2018**, *43*, 19559–19566. [[CrossRef](#)]
33. Liu, J.; Hou, J.; Xu, J.; Liu, H.; Chen, G.; Zhang, J. Ab initio study of the molecular hydrogen occupancy in pure H₂ and binary H₂-THF clathrate hydrates. *Int. J. Hydrogen Energy* **2017**, *42*, 17136–17143. [[CrossRef](#)]
34. Florusse, L.J.; Peters, C.J.; Schoonman, J.; Hester, K.C.; Koh, C.A.; Dec, S.F.; Marsh, K.N.; Sloan, E.D. Stable low-pressure hydrogen clusters stored in a binary clathrate hydrate. *Science* **2004**, *306*, 469–471. [[CrossRef](#)]
35. Lenz, A.; Ojamäe, L. Structures of the I-, II- and H-methane clathrates and the ice–methane clathrate phase transition from quantum-chemical modeling with force-field thermal corrections. *J. Phys. Chem. A* **2011**, *115*, 6169–6176. [[CrossRef](#)]
36. Becke, A.D. A multicenter numerical integration scheme for polyatomic molecules. *J. Chem. Phys.* **1988**, *88*, 2547–2553. [[CrossRef](#)]
37. Lee, C.; Yang, W.; Parr, R.G. Development of the colle-salvetti correlation-energy formula into a functional of the electron density. *Phys. Rev. B* **1988**, *37*, 785–789. [[CrossRef](#)]
38. Delley, B. Ground-state enthalpies: Evaluation of electronic structure approaches with emphasis on the density functional method. *J. Phys. Chem. A* **2006**, *110*, 13632–13639. [[CrossRef](#)]
39. Tkatchenko, A.; Scheffler, M. Accurate molecular van der waals interactions from ground-state electron density and free-atom reference data. *Phys. Rev. Lett.* **2009**, *102*, 073005. [[CrossRef](#)]
40. Cox, S.J.; Towler, M.D.; Alfè, D.; Michaelides, A. Benchmarking the performance of density functional theory and point charge force fields in their description of sI methane hydrate against diffusion Monte Carlo. *J. Chem. Phys.* **2014**, *140*, 174703. [[CrossRef](#)]
41. Parr, R.G.; Donnelly, R.A.; Levy, M.; Palke, W.E. Electronegativity: The density functional viewpoint. *J. Chem. Phys.* **1978**, *68*, 3801–3807. [[CrossRef](#)]
42. Parr, R.G.; Pearson, R.G. Absolute hardness: Companion parameter to absolute electronegativity. *J. Am. Chem. Soc.* **1983**, *105*, 7512–7516. [[CrossRef](#)]
43. Parr, R.G.; Szentpály, L.V.; Liu, S. Electrophilicity index. *J. Am. Chem. Soc.* **1999**, *121*, 1922–1924. [[CrossRef](#)]
44. Terleczyk, P.; Nyulászi, L. Dft study of possible lattice defects in methane-hydrate and their appearance in ¹³C NMR spectra. *Chem. Phys. Lett.* **2010**, *488*, 168–172. [[CrossRef](#)]
45. Verma, C.; Lgaz, H.; Verma, D.K.; Ebenso, E.E.; Bahadur, I.; Quraishi, M.A. Molecular dynamics and Monte Carlo simulations as powerful tools for study of interfacial adsorption behavior of corrosion inhibitors in aqueous phase: A review. *J. Mol. Liq.* **2018**, *260*, 99–120. [[CrossRef](#)]
46. Andersen, H.C. Molecular dynamics simulations at constant pressure and/or temperature. *J. Chem. Phys.* **1980**, *72*, 2384–2393. [[CrossRef](#)]

47. Berendsen, H.J.C.; Postma, J.P.M.; van Gunsteren, W.F.; DiNola, A.; Haak, J.R. Molecular dynamics with coupling to an external bath. *J. Chem. Phys.* **1984**, *81*, 3684–3690. [[CrossRef](#)]
48. Ewald, P.P. The calculation of optical and electrostatic grid potential. *Ann. Phys.* **1921**, *64*, 253–287. [[CrossRef](#)]
49. Sun, H. COMPASS: An ab initio force-field optimized for condensed-phase applications—Overview with details on alkane and benzene compounds. *J. Phys. Chem. B* **1998**, *102*, 7338–7364. [[CrossRef](#)]
50. Rigby, D.; Sun, H.; Eichinger, B.E. Computer simulations of poly(ethylene oxide): Force field, pvt diagram and cyclization behaviour. *Polym. Int.* **1997**, *44*, 311–330. [[CrossRef](#)]
51. Sun, H.; Ren, P.; Fried, J.R. The COMPASS force field: Parameterization and validation for phosphazenes. *Comput. Theor. Polym. Sci.* **1998**, *8*, 229–246. [[CrossRef](#)]
52. Bedrov, D.; Borodin, O.; Smith, G.D. Molecular dynamics simulation of 1,2-dimethoxyethane/water solutions. 2. Dynamical properties. *J. Phys. Chem. B* **1998**, *102*, 9565–9570. [[CrossRef](#)]
53. Martos-Villa, R.; Francisco-Márquez, M.; Mata, M.P.; Sainz-Díaz, C.I. Crystal structure, stability and spectroscopic properties of methane and CO₂ hydrates. *J. Mol. Graph. Model.* **2013**, *44*, 253–265. [[CrossRef](#)] [[PubMed](#)]



© 2019 by the authors. Licensee MDPI, Basel, Switzerland. This article is an open access article distributed under the terms and conditions of the Creative Commons Attribution (CC BY) license (<http://creativecommons.org/licenses/by/4.0/>).